Journal of Power Sources 235 (2013) 148–158

Contents lists available at SciVerse ScienceDirect

Journal of Power Sources

journal homepage: www.elsevier.com/locate/jpowsour

Expanding the Peukert equation for battery capacity modeling through inclusion of a temperature dependency

Austin Hausmann*, Christopher Depcik

Department of Mechanical Engineering, University of Kansas, 1501 W. 15th St, 3138 Learned Hall Lawrence, KS 66045, USA

HIGHLIGHTS

- The shortcomings of Peukert's battery capacity model are discussed.
- The need for a simplistic and accurate battery state of charge model is outlined.
- An efficient and capable test setup is demonstrated.
- The resulting model yields promising accuracy through minimal data requirements.

ARTICLE INFO

Article history:
Received 22 August 2012
Received in revised form
22 January 2013
Accepted 23 January 2013
Available online 9 February 2013

Keywords:
Peukert
Battery
Capacity
Modeling
Lithium
Temperature

ABSTRACT

The accuracy of Peukert's equation for battery capacity lessens under dynamic loading and varying temperature conditions. Previous attempts by others endeavor to overcome the current shortfall; however, many still neglect the inclusion of a temperature dependency. This paper investigates the feasibility of Peukert's equation for practical automotive situations and expands upon the equation in order to include both variable current and temperature effects. The method proposed captures these requirements based on the theory that a battery contains a relative maximum absolute capacity, different from manufacturer 20-h specifications, and the specific discharge conditions determine the rate at which to remove this capacity. Experimental methods presented in the paper provide an economical testing procedure capable of producing the required coefficients in order to build a high-level, yet accurate state of charge prediction model. Finally, this work utilizes automotive grade lithium-based batteries for realistic outcomes in the electrified vehicle realm.

1. Introduction

In 1897, Wilhelm Peukert tested lead-acid batteries at a constant current and determined that a single equation could be used to relate the capacity of the battery, C_P in A h, to its discharge rate [1,2]:

$$C_P = I^k \cdot t \tag{1}$$

where t is the time in hours, I is based on the constant discharge rate relative to one-ampere, and k is a calibrated, dimensionless constant. It is worth noting that in this form, Peukert's equation (often referred to as a "Law") presents a unit imbalance. The intent of this equation is to account for the intrinsic losses associated with discharging batteries at elevated currents. In particular, when discharging a battery at increasingly higher currents, the internal cell resistance increases and the recovery rate of cells decreases [1,3]. Later efforts by Pavlov demonstrated that the decrease in recovery rate is due to degradation in the number of active sites in the positive active material, as well as an increase in the resistance between the positive active material and the electrolyte [4]. The exponent, k, became known as Peukert's constant and is designed to account for these losses [5]. A value close to one represents a well-performing, efficient battery and will increase as the cell efficiency decreases [1].

It is often useful to look at Peukert's equation in terms of discharge time relative to the rated discharge time (H) [5]. Reformulation to a known capacity and discharge condition yields:

$$t = H\left(\frac{C}{IH}\right)^k \tag{2}$$

where the battery capacity, C, is generally specified as a 20-h rate from the manufacturer. This provides a better indication of

* Corresponding author. Tel.: +1 785 840 7693.
E-mail address: austin.hausmann@gmail.com (A. Hausmann).

0378-7753/$ – see front matter © 2013 Elsevier B.V. All rights reserved.
http://dx.doi.org/10.1016/j.jpowsour.2013.01.174

Nomenclature

C	rated capacity at specified discharge rate [A h]
C_d	discharged capacity [A h]
C_n	nominal capacity [A h]
C_P	Peukert capacity [A h]
C_r	capacity remaining [A h]
ΔC_r	change in capacity remaining [A h]
H	rated discharge time [h]
I	current draw [A]
I_{eff}	effective current draw [A]
I_{nom}	nominal current draw [A]
I_{ref}	reference current [A]
k	Peukert's constant [−]
R	resistance [Ω]
T	battery temperature [K]
T_{ref}	reference temperature [K]
t	time [s, h]
Δt	change in time [s, h]
V	battery voltage [V]
α, γ	current coefficients [−]
β	temperature coefficient [−]

estimated runtime; however, the equation continues to require a constant discharge current. Of importance, the authors will utilize this C nomenclature later in this effort when describing the experimental tests employed.

Doerffel and Sharkh explain that the Peukert equation cannot be used to predict remaining capacity accurately unless the battery is discharged at a constant current and constant temperature [5]. In many real world situations, batteries discharge at varying currents and experience a wide array of temperatures. This is particularly true of electrified (hybrid, plug-in hybrid, and battery electric) vehicles, a primary interest of the authors. Quite often, the Peukert equation is used in power monitoring and supply systems [6,7]; however, the drawbacks associated with more dynamic discharge environments present challenges for this model. The error introduced by attempting to model a dynamic load can be quite substantial, as the average discharge current does not accurately represent the discharge profile. For example, Rakhmatov et al. found the error associated with this runtime calculation is often more than 20% and even as high as 100% [6]. In addition, it has been documented that a battery undergoing high discharge currents can be modeled as empty using Peukert's equation, but still have energy remaining at lower discharge currents [1,3,5,8].

When considering an application such as an electrified vehicle, the discharge time is typically much shorter (one to eight hours) than that of power monitoring or backup systems. An alternative method of using Peukert's equation for varying current is based on a rolling average technique in order to calculate the average discharge current over a previous time span and assume this value as constant over the same given time span [9,10]. However, this method can result in a simulated current draw even though no energy is physically being removed [5]. Another generally accepted form for improving Peukert's equation utilizes variable current calculated as a pseudo-effective current (I_{eff}) [11,12]:

$$I_{eff} = I\left(\frac{I}{I_{nom}}\right)^{k-1} \tag{3}$$

where I is the actual discharge current and I_{nom} is the nominal current relating to the manufacturer supplied capacity (typically the 20-h discharge rate).

In both alternative methods, use of the effective discharge current allows calculation of the total capacity removed from the battery:

$$C_d = \sum\left(I_{eff} \cdot \Delta t\right) \tag{4}$$

where the capacity discharged (C_d) is the total capacity removed from the battery based on the effective current over time. Thus, the capacity remaining (C_r) is equal to the nominal capacity (C_n), given by the manufacturer as a 20-h discharge rate, minus the capacity discharged:

$$C_r = C_n - C_d \tag{5}$$

Both methods have been known to show improved estimation of discharge capacity for varying current discharge [5,6]; however, both solutions also neglect temperature effects.

Of interest for this work, lithium-based batteries typically demonstrate higher ion transport between the electrode and electrolyte as compared to other battery technologies, such as lead-acid [13]. This rate increase allows lithium-based batteries to be discharged at relatively higher rates with less loss of performance, resulting in higher cell efficiencies and, thus, reduced values for k (closer to one). Another interesting aspect of lithium batteries is the relatively flat voltage profile throughout the discharge. While this aspect provides a more constant power source than a typical lead-acid battery, it hinders the ability to measure battery State of Charge (SOC) using voltage. Current methods for state of charge modeling use a combination of Coulomb counting (measuring the current at each time step and summing the values to achieve capacity) and voltage profiles to achieve a state of charge profile. However, this method makes accounting for losses difficult and has known accuracy issues [1].

Batteries of all chemistries demonstrate varying available capacities for different temperature profiles [1,3,14–16]. As the battery temperature decreases, the available capacity decreases due to retardation of the chemical metabolism of the cells effectively hindering the chemical reaction rate [1]. This aspect is completely disregarded in Peukert's equation and can lead to significant errors for even slight changes in environmental conditions or battery self-heating effects [5,17]. For example, Gao et al. [16] demonstrates this temperature relationship for lithium-ion battery cells as illustrated

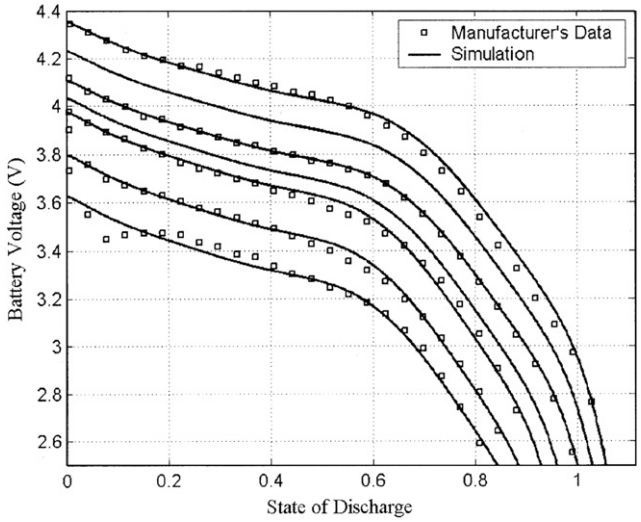

Fig. 1. Gao et al. data for lithium-ion capacity and temperature relationship, at temperatures of (top to bottom) 45 °C, 34 °C, 23 °C, 10 °C, 0 °C, −10 °C, −20 °C at a discharge current of 0.7 A [16].

Table 1
Physical specifications of investigated automotive grade lithium battery cells.

Manufacturer & chemistry	Surface area [cm^2]	Mass [g]
CALB $LiFePO_4$	1098	3256
ThunderSky $LiFePO_4$	1040	3018
Headway $LiFePO_4$	1433	3700
Kokam LiPO	1445	1301

in Fig. 1. As a result, Peukert's equation only holds valid at room temperature while also assuming a constant discharge rate.

While several authors demonstrate empirical test results [18–22], there is a relatively limited amount of information within the literature for dynamic battery capacity temperature modeling using automotive grade batteries. The most accurate models include electrochemical processes in order to define battery performance [22,23]. The use of such a model can correctly encompass numerous battery characteristics, such as electrode geometries, concentration of the electrolyte, diffusion coefficients, transfer coefficients, reaction rate coefficients, and other lower-level phenomena [22–30]. Hence, while the creation of an electrochemical model is likely more exact in its predictions and can provide better results, the creation, calibration, and implementation of such models requires significant computational capabilities. This makes these simulations less suitable for on-road vehicular battery prediction. Additionally, the extensive effort spent on such models can quickly become inapplicable if the system in question requires a change in cell chemistry or configuration since calibration of the models happens via a specific battery and pack configuration. As a result, the majority of these models requires either widespread calibration, exhaustive computational resources, or fails to tune the models for dynamic discharge conditions limiting their effectiveness in mobile applications.

As an alternative to electrochemical endeavors, analytical, physically-based simulations often provide the necessary accuracy without the calibration and chemical kinetic modeling [23]. The work of Gao et al. [16] accurately models not only temperature effects through analytical methods, but also dynamic current and cell resistance. However, this effort requires data storage of multiple measurements throughout the time-history of a discharge cycle, as well as numerical integration using numerous variables at each time-step. Similar efforts by Peck and Pierce [22] only consider static discharge current and ignore effects of cell chemistry and cell design. While analytical methods of this magnitude are simpler and more adaptable than electrochemical models, they remain computationally intensive and require the use of an auxiliary computing system beyond that of a typical smart battery system or battery management system [23]. Furthermore, even simpler analytical models calibrated by cell chemistry also exist [31–34]. Often these models are calibrated by testing cells over a large matrix of constant current and constant temperature discharge conditions [31]. For example, Gold produced a macromodel that accounts for thermal capacity effects through cell resistance, ambient temperature, and heat capacity. However, of the three, only ambient temperature is modeled as dynamic [33]. While these approaches can often be appropriate for controlled condition discharging, they do not necessarily apply to the highly dynamic world of electrified automobiles.

In an effort to facilitate a numerically efficient model for battery capacity estimation at different currents and temperatures, the following sections describe and validate an update to Peukert's equation. First, this work presents the derivation of the model illustrating the current and temperature dependencies. Then, the next section describes the experimental tests performed using commercial, automotive-grade lithium battery chemistries. Finally, simulation of these batteries based on dynamic current draw and battery temperature demonstrates model capabilities.

2. Improved model

In order to improve Peukert's equation, this work proposes an alternative definition of available capacity. Traditionally, manufacturers define the capacity of the battery for various discharge times, such as the 20-h rate (e.g., Eq. (2)). This concept proves confusing as it provides different values for battery capacity based on the usage profile [5]. Under high loading conditions, a battery may demonstrate empty conditions via the low voltage cutoff. However, this battery still has capacity that may be utilized at lower discharge rates [1,3,5,26]. This characteristic can lead to ambiguity as to how much capacity actually remains. As a result, this effort assumes that a battery will always contain a remaining maximum available capacity (C_r). This capacity remains uniform regardless of the discharge conditions; however, the specific conditions during discharge influence the rate of discharge. Since the assumption involves an absolute maximum capacity remaining, capacity reaches zero at 100% depth of discharge and can never fall below this zero value. In order to account for various discharge criteria effects, the conditions of the discharge routine influence the discharge rate as follows:

$$C_r^{t+1} = C_r^t - \Delta C_r \tag{6}$$

where C_r^0 is an absolute capacity of a fully charged battery (zero percent depth of discharge) at time equal to zero.

As previously mentioned, this discharge rate is primarily dependent on the discharge current (I) and battery temperature (T) at each time t:

$$\Delta C_r = f(I, T) \tag{7}$$

When battery temperature decreases and load increases, the rate at which the capacity is reduced also increases. A constant (α), analogous to Peukert's constant, models the dynamic current (I_t) in amperes relative to a reference current (I_{ref}):

$$f(I) = \left(\frac{I_t}{I_{ref}}\right)^{\alpha} \tag{8}$$

Conditions similar to Peukert's law should control this exponent, as long as one uses Peukert's one-ampere reference current as the authors have accomplished.

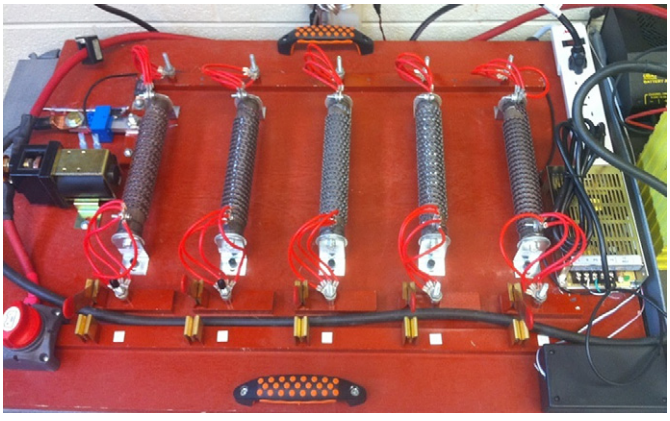

Fig. 2. Variable resistive load bank constructed to discharge batteries under adjustable currents.

Fig. 3. Cold chamber picture of CALB 90 A h prismatic battery inside chamber and connections on outside of chamber.

In order to account for temperature dependency in K, a similar term is used:

$$f(T) = \left(\frac{T_{\text{ref}}}{T_{\text{t}}}\right)^{\beta} \tag{9}$$

The exponent (β) drives the temperature relationship and is reliant on the battery chemistry and on the physical specifications of the battery cells, and on its pack configuration. In this form, β will provide an indication of how well the battery responds to thermal changes on either side of the reference temperature. Based on the work by Gao et al. (Fig. 1), the temperature–capacity relationship for lithium-ion cells appears to be reasonably linear for higher temperatures, but it is non-linear at lower temperatures. Furthermore, Buchmann explains that this relationship can be approximated as linear [1], however Gold states that the relationship is non-linear throughout the entire operating range [33].

Since these formulations are dimensionless and the capacity removed from the battery at time t is in A h, a constant (γ) in A h relates the capacity removed to the non-dimensional discharge current and temperature components. As a result, the final form for instantaneous capacity removed is:

$$\Delta C_{\text{r}} = \gamma \cdot \left(\frac{I_{\text{t}}}{I_{\text{ref}}}\right)^{\alpha} \cdot \left(\frac{T_{\text{ref}}}{T_{\text{t}}}\right)^{\beta} \tag{10}$$

This equation illustrates from a physical standpoint that, as the discharge current increases, the effective capacity removed will increase. This correlation is in accordance with the commonly-used Peukert equation reasoning. However, the model now demonstrates that, as the temperature of the battery decreases, the effective capacity removed also increases. The literature in this area illustrates this relationship [1,3,5,8,16,17]; however, the exact order of the correlation is debatable and requires verification experimentally.

3. Experimental work

Electric drive vehicles undergo relatively dynamic operating situations in which the discharge current and operating conditions can change dramatically over the course of a cycle. From an application standpoint, electrified vehicles would be a primary benefactor of an improved battery capacity model. The typically limited onboard computing abilities associated with vehicular computing would benefit from a model with low memory and processing requirements. Due to the status of lithium-based battery technology, this study investigates testing of this chemistry in various forms of automotive grade battery packaging [1,35,36]. In specific, this effort tests the following chemistries, cell designs, and manufacturer-specified 20-h capacities:

Fig. 4. Heated test enclosure with ThunderSky 90 A h prismatic cell.

- CALB (CALB, Inc., Luoyang, China) NSA 100 Lithium Iron Phosphate ($LiFePO_4$), 100 A h prismatic cell
- ThunderSky (Winston Global Energy Limited, Shenzhen, China) LFP90 Lithium Iron Phosphate ($LiFePO_4$), 90 A h prismatic cell
- Headway (Zhejian Xinghai Energy Technology Co., Ltd., Zhejiang Province, China) 38140S Lithium Iron Phosphate ($LiFePO_4$), 100 A h cylindrical cell package (1S10P)
- Kokam (Dow Kokam, Midland, Michigan, United States of America) SLPB96255255 Lithium Cobalt Dioxide ($LiCoO_2$), 60 A h pouch cell

The cells chosen provide the ability to investigate the effects of the cell design, specific chemistry, and nominal capacity on overall cell performance. While all cells are representative of typical automotive batteries, the physical design varies from cell to cell, most noticeably in weight and surface area as seen in Table 1.

Tests are run for over two cells of each type in order to account for the possibility of individual cell performance variation. Moreover, in order to capture the effects of varying current and temperature, the following test conditions are used:

- 0.5 C discharge current at chilled, room, and hot conditions
- 1.0 C discharge current at chilled, room, and hot conditions
- 3.0 C discharge current at chilled, room, and hot conditions

with the discharge current ratings (C-ratings) based on the manufacturer specified 20-h capacity that will be discussed later in more depth. These conditions are representative of the operating ranges typically provided by cell manufacturers and provide a normalized approach to discharge currents with varying cell capacity. The given testing matrix effectively tests four unique lithium-based battery designs against nine separate test criteria.

Cells are electrically loaded using a custom-built resistive load bank presented in Fig. 2. The load bank consists of five resistors

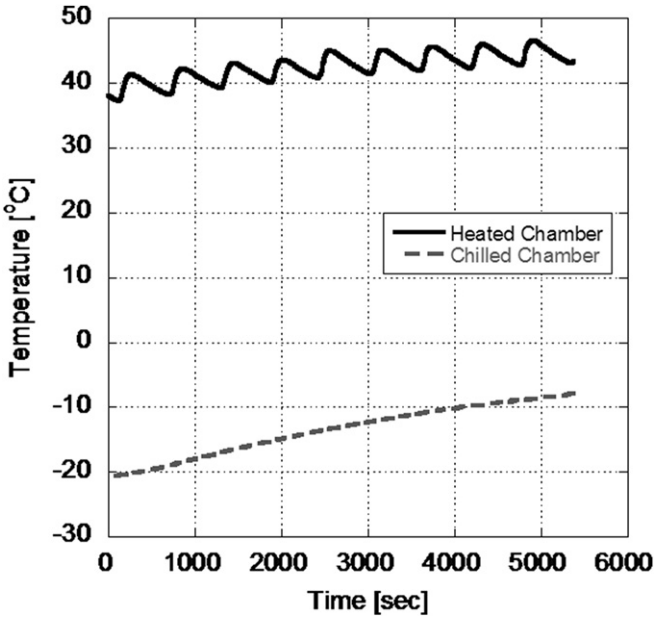

Fig. 5. Example test profiles for the chilled and heated chambers.

(300-W Power Series from Milwaukee Resistor Corporation, Milwaukee, Wisconsin, United States of America) wired in parallel with the ability to add each one individually using knife switches. When applied to a 3.3-V cell, this provides for the ability to test various currents from 6 to 330 A over the resistor range of 0.01–0.5 Ω. As a result, this resistive load bank provides a variable loading experiment by virtue of Ohm's Law:

$$I = \frac{V}{R} \tag{11}$$

where V is the cell voltage and R is the resistance of the setup employed during the test.

Due to the high accuracy (>99%) and excellent thermal capabilities ($\leq 3 \times 10^{-6}\ \Omega/°C$) of the resistors, the applied resistance remains relatively constant throughout the duration of the test. As a result, when the battery voltage drops under load, the applied current additionally drops providing a dynamically varying loading situation that Peukert's equation cannot handle. This aspect requires that the proposed model account for a varying current in order to predict the battery SOC accurately at any point during the discharge cycle.

It is important to note that use of constant resistive loads makes defining the discharge currents relative to the nominal manufacturer capacity of the cells difficult. As expressed via Ohm's law, when the voltage of the cell drops due to loading, the current draw through the resistive load bank also decreases. This makes it problematic to apply the exact resistance that will result in a 0.5 C, 1 C, or 3 C average load. Since the process of choosing the appropriate resistor is circular (as the resistance changes, the current also changes; therefore, this changes the voltage drop under load requiring another resistor change), the load will change throughout the course of the test. To maintain simplicity, the authors chose specific resistances for the 0.5 C, 1 C, and 3 C loads that apply the desired load under open-circuit voltage conditions assuming no voltage drop when loaded. While this does not result in true 0.5 C, 1 C, and 3 C loads, it maintains relative discharge criteria consistent for all of the cells.

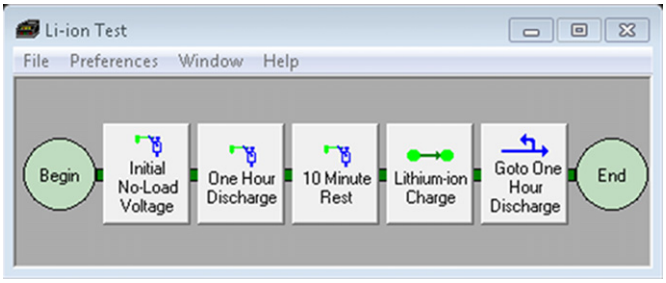

Fig. 6. Sample battery analysis routine (BAR) graphical representation for Vencon UBA-5.

Chilled testing occurs by placing the battery in a small medical grade freezer (Summit FS20L7, Summit Appliance, Bronx, New York, United States of America) while allowing it to soak overnight to approximately −20 °C. This is typically the lower operating limit of most lithium cells, as well as the lower limit of the freezer. The freezer door includes contact terminals in order to allow for connection of the load bank and voltage sensors without compromising the enclosure seal (Fig. 3). The battery remains in the freezer with the compressor running for the entire duration of the test. As the test progresses, the battery temperature increases due to ohmic heating, heat generation due to entropy change, phase change, heat capacity change, and other phenomena [37]. A portion of this heat generation transfers convectively to the environment raising the temperature of the test chamber. This functionality allows the test to be performed using dynamically changing temperature similar to that of a real would situation. From a vehicular application standpoint, this test is representative of the battery pack initially cold soaked from being parked outside for the evening with subsequent self-heating as the driver starts and completes his or her route.

To perform heated testing, the battery is placed in a fiberglass insulated, electrical enclosure with a TEMPCO (Tempco Electric Heater Corporation, Wood Dale, Illinois, United States of America) EHT00038 500-W enclosure heater (Fig. 4). The heater is equipped with a thermostat that allows the internal temperature to cycle between 37 °C and 41 °C. As the test progresses, the battery not only experiences the cyclic temperature changes due to the thermostat's characteristics, but also sees the magnitude of these cycles increasing due to heat released by the battery. Similar to the chilled testing, this allows the test to be performed using dynamically changing temperature similar to that of a real world situation. Fig. 5 provides example temperature profiles for the heated and chilled test chambers. Finally, ambient temperature testing occurs at roughly 25 °C in an open-air environment. Thermal changes for this test are simply a result of the battery temperature rise due to loading conditions.

This work utilizes a Vencon (Vencon Technologies Inc., Toronto, Canada) UBA-5 commercial battery analyzer for capture of experimental test data. The UBA-5 operates via a personal computer while monitoring and logging the results of the test at one-second intervals. Voltage measurement accuracy is in thousandths of a volt and acts as the termination criteria for the test at the manufacturer-

Table 2
Voltage operational limits of the investigated cells as specified by the manufacturer.

Manufacturer & chemistry	Low voltage cut-off [V]	Upper voltage limit [V]
CALB $LiFePO_4$	2.50	3.60
ThunderSky $LiFePO_4$	2.50	4.25
Headway $LiFePO_4$	2.00	3.65
Kokam LiPO	2.70	4.20

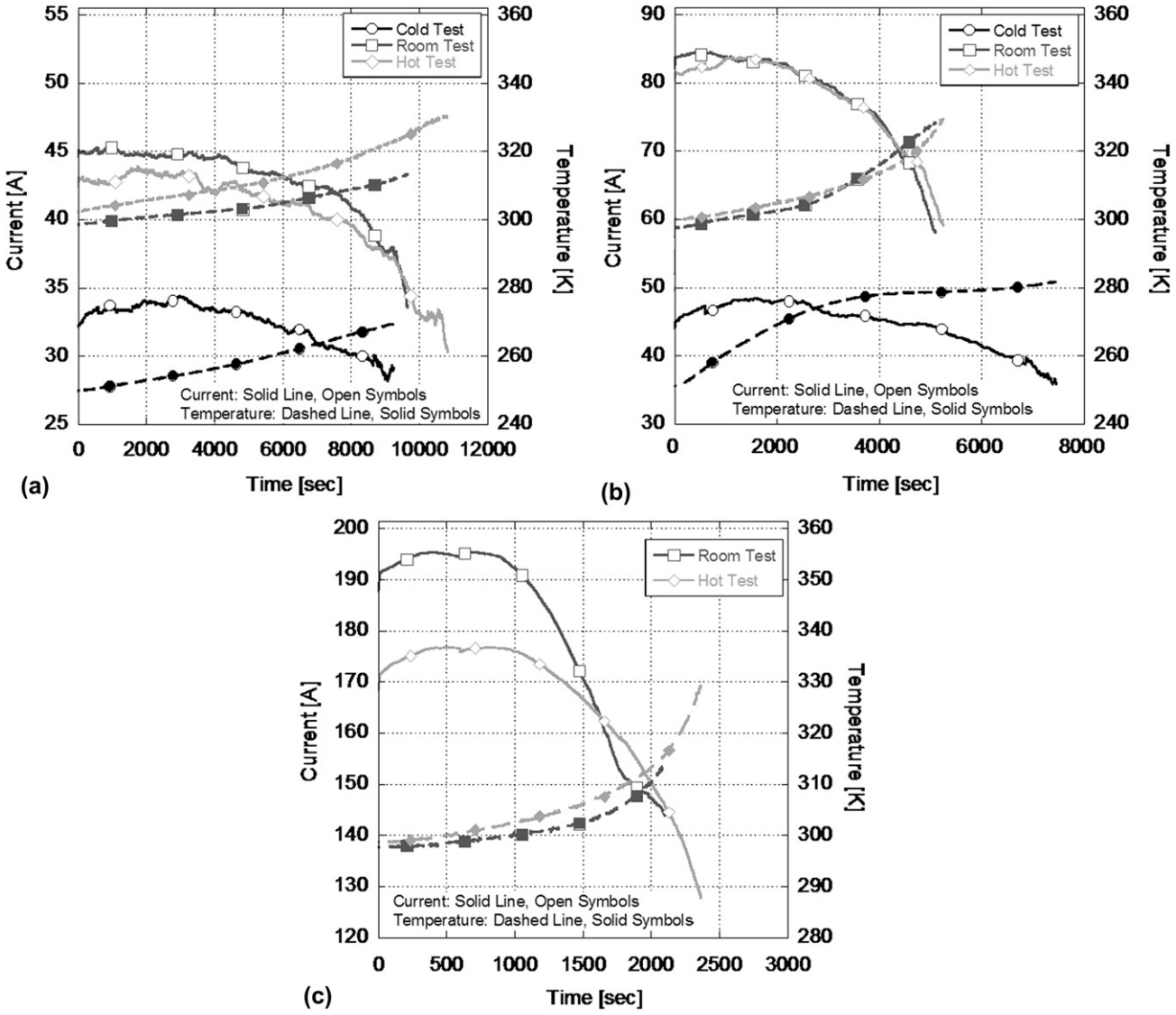

Fig. 7. Headway cell #1 dynamic current and temperature profiles for a) 0.5 C, b) 1 C, and c) 3 C discharge rates.

specified low voltage cutoff of the battery. Results files containing the entire test data are output as comma separated values (CSV) format for input into data analysis programs. Each of the cells tested utilize a custom-built battery analysis routine (BAR) in order to ensure proper test termination. BARs are setup using graphical representations of the testing algorithm applied by the UBA-5. These algorithms produce the necessary commands for the UBA-5 throughout the progression of a test based on a variety of set parameters and limits (Fig. 6).

For this study, simplistic battery analysis routines were setup using only discharge criteria with the appropriate low-voltage cutoff (Table 2). This allows the UBA-5 to begin collecting data as soon as the test is started by the user and automatically terminates the load and data collection once the termination criteria is reached. Each cell type employs a specific BAR by changing the test termination condition in the default lithium discharge BAR. While the UBA-5 is capable of charging the cells after test completion, this is performed using separate chargers (discussed later) to free up the UBA-5 for additional testing.

Battery temperature data was recorded at the same time intervals as all other performance data using two calibrated Philips (Philips Electronics N.V., Amsterdam, Netherlands) SN74LS04 model thermistors. In its commercially available form, the UBA-5 only allows temperature monitoring above 0 °C. While the thermistors are capable of monitoring down to −30 °C, Vencon calibrates their range using a specified pull-down resistor for temperatures varying from 0 °C to 100 °C in order to maintain linearity between voltage and temperature. With the technical assistance of Vencon [38], this pull-down resistor was replaced with the appropriate resistor that allows one of the thermistors to be used at temperatures as low as −30 °C. This required changing the required UBA-5 calibration file in order to match the new resistance value. The remaining thermistor kept its original configuration for the room and elevated temperature tests.

The direct current measuring capabilities of the UBA-5 are limited to 3.0 A per channel. In order to measure higher current values accurately, a Tamura (Tamura Corporation of America, Escondido, California, United States of America) model L03S300 hall-effect current transducer is used. This current transducer outputs the system current to one of the 0–5 V analog inputs on the UBA-5 device. This conversion occurs in the data analysis script in order to refer the voltage readings back to the corresponding current draw.

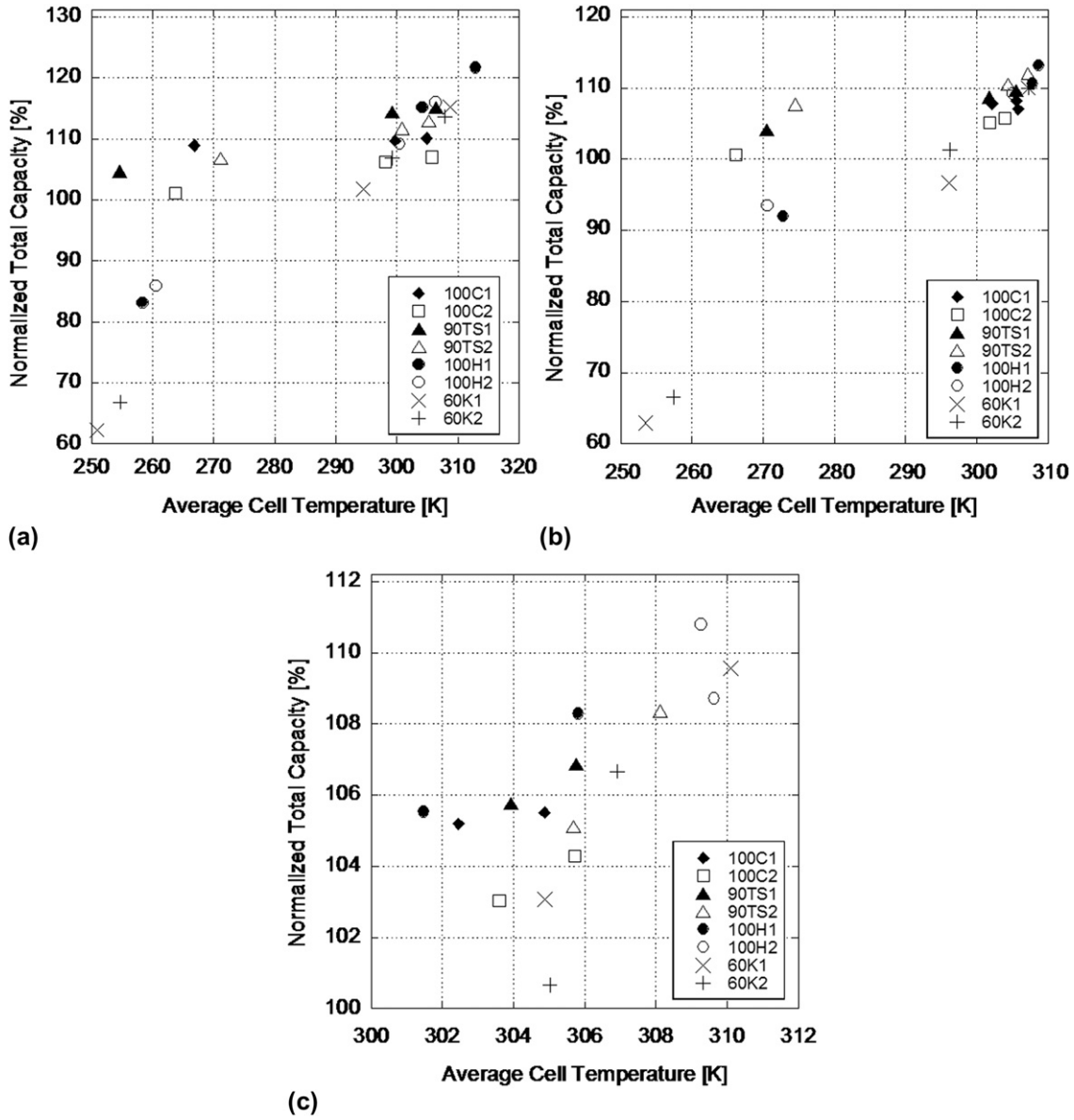

Fig. 8. Normalized total capacity with respect to cell temperature for a) 0.5 C, b) 1 C, and c) 3 C discharge rates.

After testing, the authors allow the battery to return to room temperature before charging according to manufacturer's specifications. In particular, a Venom (Vertical Partners West, Rathdrum, Indiana, United States of America) model 0660 intelligent charger ensures appropriate and consistent charging conditions. It allows for charging multiple cell chemistries using a constant-current, constant-voltage algorithm. This permits unattended charging while ensuring fully charged cells without overcharging. Table 2 lists the upper and lower voltages used for testing and charging.

4. Results and discussion

With respect to results, the recording of data signals happened at a 1-Hz rate with the exception of current that was limited to 0.25 Hz because of the update rate of the Hall-effect current sensor. MATLAB (MathWorks, Inc., Natick, Massachusetts, United States of America) provided for the numerical framework of compiling and analyzing the data obtained during the experimental tests. In order to ensure the data are aligned properly and to reduce the noise effects of the signals, a 1-D digital filter is applied using MATLAB (from MATLAB manual: direct form II transposed implementation of standard difference equation [39]). Use of the filter outside of an iterative loop allows for a running average of the data set along with estimation of the pack current on a per second basis. Moreover, while the intent was to test all cells at three temperature conditions for all discharge profiles, the performance of all four cells prohibited testing under cold, 3 C discharge conditions. In this case, when the cell was loaded, its voltage dropped below the low-voltage cut-off of the respective cell. As a result, the authors did not perform these tests in order to prevent cell damage.

The basic principle of the proposed model is the ability to calculate capacity effects for varying temperature and current during the discharge cycle of a battery. As an example of the dynamic conditions the cells encounter during testing, Fig. 7 indicates the current and temperature for all eight individual tests of Headway cell #1. Moreover, in an effort to expand upon the basic Peukert model, the proposed model must capture the effects of

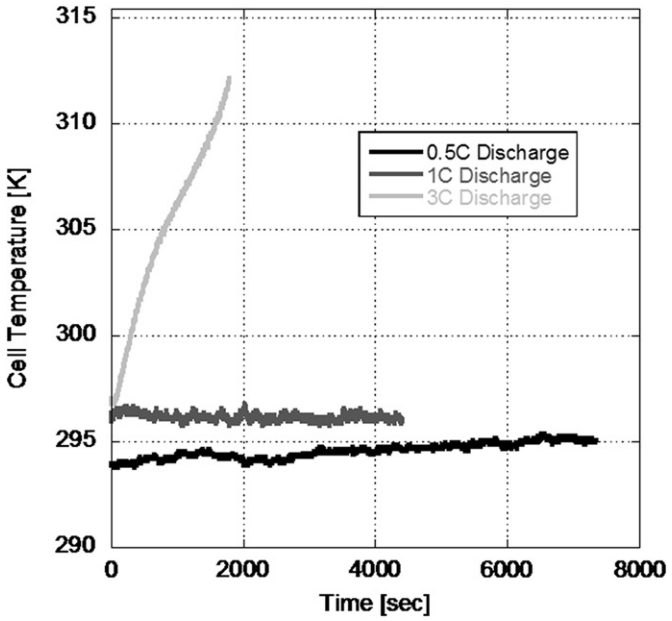

Fig. 9. Kokam cell #1 battery temperature profiles under different discharge conditions during an ambient test.

temperature on the available capacity of the cell. Fig. 8 demonstrates the effects of cell temperature on discharge capacity.

Grouping of data in Fig. 8 with respect to the loading conditions helps to emphasize the temperature effects upon discharging. Note that normalized total capacity is a measure of the available capacity over manufacturer specifications given the particular discharge conditions; e.g., 110% for the Kokam cells would indicate that the battery has an effective capacity of 66 A h during the defined experiment. As the average temperature of the cell increases, the total capacity of the cell also increases. The results match theoretical expectations [1,16,33] and make sense physically. As the cell temperature increases, the internal resistance of the cell decreases and the chemical metabolism of the cell increases, effectively increasing the capacity of the battery [1].

Developing similar trends based on current draw proves difficult, largely due to the non-linearity and complexity of the applied testing conditions. A 0.5 C test would result in a higher total capacity than a 3 C test at the same temperature due to Peukert effects; however, the increase in cell temperature during the faster discharge event has the potential to outweigh this influence (recall Fig. 8 where capacity goes up with temperature). This is especially true during cold chamber testing where nearly all of the cells demonstrated equal or higher total capacities at elevated discharge rates due to cell heating.

As an example, Fig. 9 presents the temperature profile for Kokam cell #1 as a function of discharge rate. The temperature increase due to the elevated loading during the 3 C discharge offsets the negative effects of the elevated current draw, resulting in a higher discharge capacity at 3 C (61.84 A h) than at 0.5 C (61.06 A h) and 1 C (57.97 A h). Using the appropriate coefficients

Table 3
Model optimization results with constant γ (1 A h), and C_r^0 (120%) in order to increase proper physical representation.

	CALB $LiFePO_4$	ThunderSky $LiFePO_4$	Headway $LiFePO_4$	Kokam LiPO
α	1.027	1.021	1.023	1.043
β	0.324	0.440	1.720	2.910

Table 4
Model optimization results for all four coefficients.

	CALB $LiFePO_4$	ThunderSky $LiFePO_4$	Headway $LiFePO_4$	Kokam LiPO
α	1.0269	1.0213	1.0287	1.0486
β	0.3072	0.4393	1.7809	2.9988
γ	1.0032	1.0047	1.0193	1.0259
C_r^0	119.80%	121.95%	126.04%	127.33%

(covered later), the 0.5 C and 1.0 C discharge tests were modeled isothermally at the average temperature of the 3 C test (305 K). The model predicted 66.08 A h of discharge capacity for the 0.5 C test and 63.98 A h for the 1 C test using the elevated temperature. As expected, both tests outperformed the actual 3 C test, as well as the modeled 3 C test (59.44 A h).

Calculation of the actual model coefficients and exponents utilizes a constrained nonlinear optimization. This particular method utilizes a least-squares fit to compare the relative discharge curve from the test data to the discharge curve generated by the proposed model at each data point (1 s intervals). For this situation, the optimization must be constrained by known bounds in order to ensure physicality of the model. For example, α is similar to the Peukert's constant and in a physical sense cannot drop below 1.0 and is rarely more than 1.5 for modern battery technology [1,3]. Providing good initial guesses and a bound that makes sense physically reduces the chance of the optimization method settling on local, erroneous minimums. The squares of the differences between the test data and model are summed and the square root of the sum is then used as the reduction term for the optimization. This optimization is done by changing the model variables until minimizing this summation to a set tolerance (10^{-6}). Ideally, the optimization finds a set of coefficients and exponents that allow this value to be equal to zero.

Again, MATLAB provides the framework for the model and optimization. MATLAB allows custom computing scripts to be created and executed utilizing a simplistic programming language with optimization toolboxes available to perform the needed analysis. The specific routine utilized for optimization in MATLAB involves the Gauss–Newton method in order to minimize the resulting final value of the function. Other methods are acceptable; however, since the Gauss–Newton method does not require the calculation of the second derivatives of the function, choice of this routine retains computational efficiency.

The authors first employed the model with a constant α and allowed the optimization routine to find γ, β, and C_r^0. Since α is known to a rough approximation ($\sim$1.03) for lithium batteries, holding it initially constant allows the optimization procedure to focus on the unknowns. This method provides an estimate of the magnitude of γ, β, and C_r^0 for the proposed model. The results of this initial iteration indicated a γ near one with a value of C_r^0 typically between 110 and 120% of the nominal capacity. From a physical standpoint, this is reasonable since γ is used to relate the model to the test data at a current draw relative to 1 A (I_{ref}) and a temperature relative to 298 K (T_{ref}). Ignoring the effects of β, the equation effectively becomes Peukert's equation (with $I_{ref} = 1$ A). The work presented here allows for some adaptation by not requiring that γ be equal to one as Peukert specifies. As a result, by subsequently setting γ equal to one in the second optimization while again holding α constant, the model can effectively move in the right direction reducing the possibilities of local minimums and finding physical values for the other coefficients. The initial test results also reveal that the actual capacity of the cells was rarely more than 120% of nominal, indicating a C_r^0 near 120% of the 20-h C rating. This optimization occurs over both cells of each type in the same optimization in order to create a set of coefficients for a particular

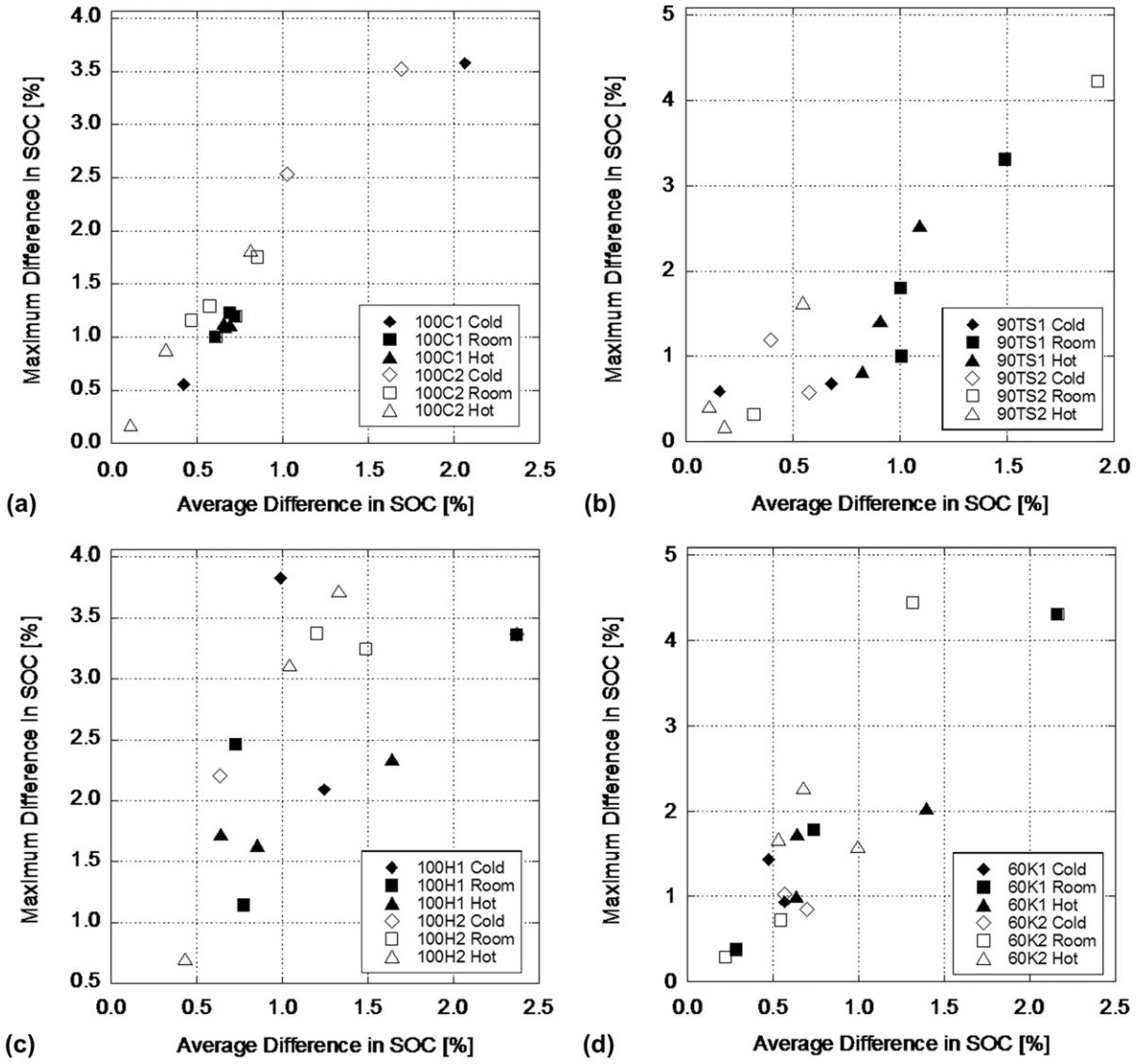

Fig. 10. Average and maximum model accuracy with respect to SOC for a) CALB, b) ThunderSky, c) Headway, and d) Kokam cells.

battery type as opposed to a set of coefficients that only matches a single, specific cell.

Utilizing the results from this method as initial values, γ is set to 1 A h and C_r^0 equal to 120% of the nominal cell capacity. This systematic approach removes some of the flexibility of a four-variable optimization and reduces the likelihood of the optimization producing a non-physically based curve-fit. Table 3 presents the results from this optimization. Using these results as initial guesses, Table 4 presents the optimization results utilizing all four variables in order to find the best fit possible.

Investigation of the overall accuracy of the model included calculated deviations between the predicted SOC for the model and actual experiment. The experimental SOC for the test is calculated as a percentage of the measured energy removed from the cell during the test. Fig. 10 illustrates the *maximum* deviation (*y*-axis) seen in the actual SOC to the model, along with the *average* difference (*x*-axis) in SOC. Representation of the plots in this manner illustrates results from all tests in an easy to digest format. The model provides close agreement with the experimental test results with all outcomes within 95% of the actual tested values. In addition, more than 80% of the tests are within 97% of the test data. Further testing to provide average discharge profiles would help refine the data; however, due to the capacity of the cells under investigation, it took six months to complete the study as-is. Future work will explore average profiles and the resultant standard deviations in the experimental tests.

By demonstrating the voltage and depth of discharge relationship for each of the tested cell types at the 0.5 C discharge rate (Fig. 11), it becomes clear that the model accurately simulates the absolute depth of discharge (DOD) across a wide variety of operating temperatures for all of the investigated cell types. When comparing the two most similar cells, CALB and ThunderSky, the CALB cells outperform the ThunderSky cells in temperature performance by a fair margin. This is to be expected as CALB was developed as a sister company of ThunderSky for use as a Chinese aviation lithium battery and is held to higher performance standards [40]. These standards may be the underlying reason for the CALB cells demonstrating some of the most desirable temperature and current coefficients (low β and γ respectively) of all the cells tested as well. Given the same discharge criteria and battery capacity, the cell design with the lower β and γ will result in the longest discharge time.

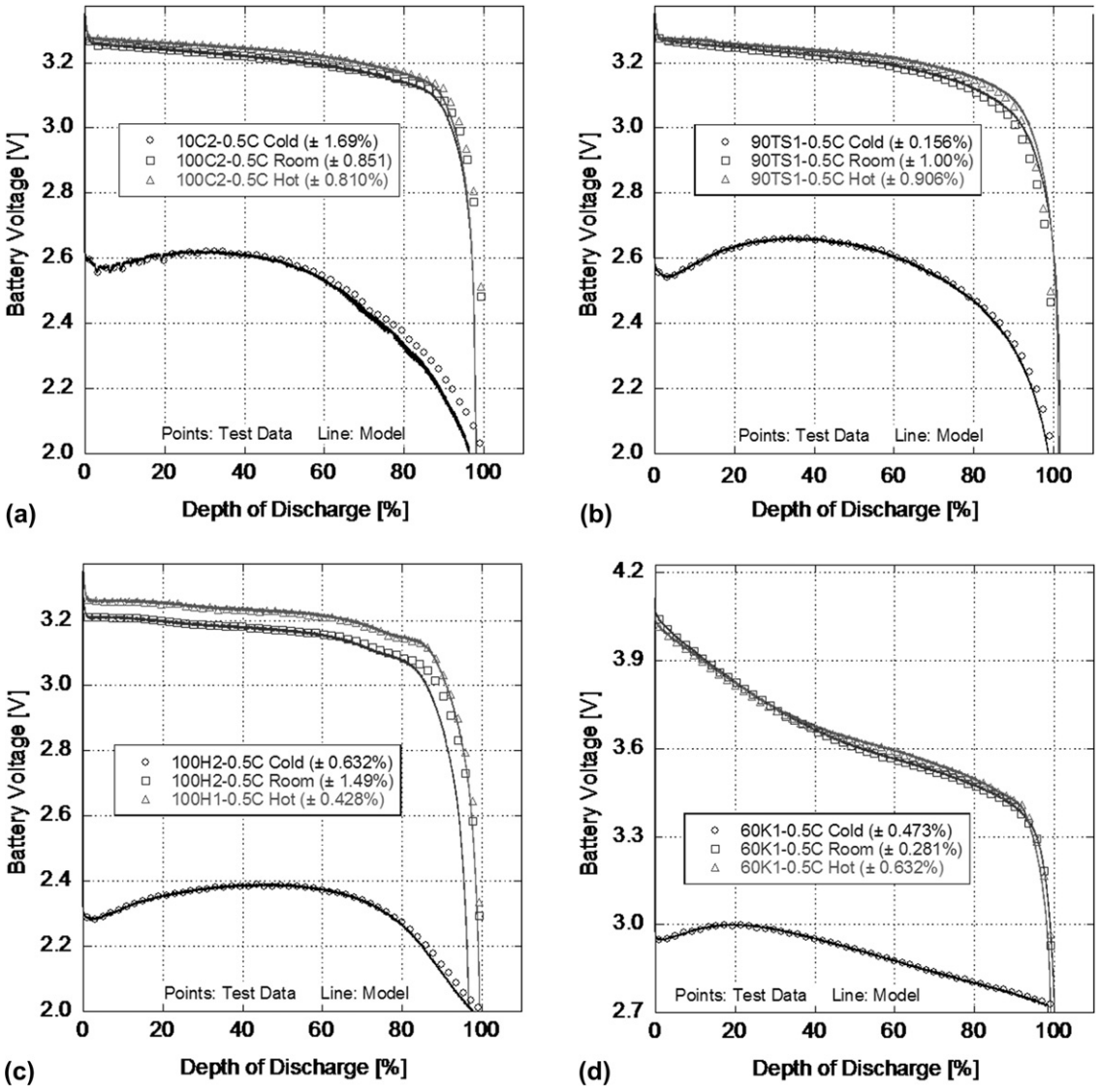

Fig. 11. 0.5 C discharge profiles with average depth of discharge error indicated for a) CALB, b) ThunderSky, c) Headway, and d) Kokam.

The Kokam pouch cells exhibit the highest increase over the manufacturers specified nominal capacity; however, these cells have the largest temperature and current coefficients of all cells tested, somewhat outweighing this benefit. This illustrates that care should be taken when performing the testing in order to ensure the battery pack design is in "end use" form as the temperature coefficient is likely dependent on the physical cell design. Due to chemistry and nominal capacity, the Kokam cells demonstrated the lowest mass and highest surface areas of all the cells tested and, as a result, environmental changes influenced these cells the most. The Headway multiple cell configuration is also the likely cause of the higher temperature coefficients value as there is a large amount of surface area between the individual cells (Fig. 12).

The test data and resulting correlations indicate battery temperature performance is not only a function of cell chemistry, but physical specifications and pack configuration as well. The model effectively captures the physical battery chemistry and the environmental effects on the overall cell design. The result is a real world battery model based on fundamental, physical relationships capable of configuration by manufacturers and system-builders alike for multiple pack designs. With that in mind, future work

Fig. 12. Cells under investigation (from left to right) CALB 100 A h, ThunderSky 90 A h, Headway 10P1S 100 A h pack (front), Kokam 60 A h.

should involve studying the use of multiple cells in closely packed configurations to explore the effect of cell density on temperature performance.

5. Conclusion

The evolution of battery technology requires a numerically efficient method to predict correctly the remaining State of Charge of batteries at any point during a discharge cycle utilizing a minimal data set. Historically, this occurs through a combination of Coulomb counting and open-circuit voltage profile interpolation algorithms. These methods make quantifying cell temperature effects difficult or non-existent.

This paper demonstrates an intuitive and comprehensive, yet high-level model that accurately predicts the remaining battery capacity to within five-percent across a wide range of operating conditions. Due to the minimal required data set and computational simplicity, the model remains feasible for the current state-of-the-art battery technology, as well as for integration within battery management systems. The test methods presented provide a straightforward and economical approach to capturing the required data set and allow future work to investigate the effects of battery pack configurations, as well as various thermal management methods.

Acknowledgments

This research was partially funded by the University of Kansas, Transportation Research Institute from Grant # DT0S59-06-G-00047, provided by the US Department of Transportation – Research and Innovative Technology Administration. Moreover, Smith Electric Vehicles additionally supported this effort.

References

[1] I. Buchmann, Batteries in a Portable World, Cadex Electronics, 2001.
[2] W. Peukert, Elektrotechnische Zeitschrift 20 (1897) 20–21.
[3] D. Linden, T.B. Reddy, Handbook of Batteries, third ed., McGraw-Hill, 2002.
[4] D. Pavlov, G. Petkova, Journal of the Electrochemical Society 149 (2002) A654.
[5] D. Doerffel, S.A. Sharkh, Journal of Power Sources 155 (2006) 395–400.
[6] D. Rakhmatov, S. Vrudhula, D.A. Wallach, IEEE Transactions on Very Large Scale Integration (VLSI) Systems 11 (2003) 1019–1030.
[7] D. Rakhmatov, S. Vrudhula, D.A. Wallach, in: Proceedings of the 2002 International Symposium on Low Power Electronics and Design (2002), pp. 154–159.
[8] M. Doyle, J. Newman, J. Reimers, Journal of Power Sources 52 (1994) 211–216.
[9] V. Johnson, Journal of Power Sources 110 (2002) 321–329.
[10] R.Y. Ying, US Patent 6646419, 2003.
[11] J. Bumby, P. Clarke, I. Forster, Physical Science, Measurement and Instrumentation, Management and Education-Reviews, IEEE Proceedings A 132 (1985) 265–279.
[12] T.B. Atwater, US Patent 5640150, 1997.
[13] J.M. Oh, O. Geiculescu, D. DesMarteau, S. Creager, Journal of the Electrochemical Society 158 (2011) A207.
[14] G. Amatucci, C. Schmutz, A. Blyr, C. Sigala, A. Gozdz, D. Larcher, J. Tarascon, Journal of Power Sources 69 (1997) 11–25.
[15] R. Rao, S. Vrudhula, D.N. Rakhmatov, Computer 36 (2003) 77–87.
[16] L. Gao, S. Liu, R.A. Dougal, IEEE Transactions on Components and Packaging Technologies 25 (2002) 495–505.
[17] J. Larminie, J. Lowry, I. NetLibrary, Electric Vehicle Technology Explained, Wiley Online Library, 2003.
[18] A. Du Pasquier, I. Plitz, S. Menocal, G. Amatucci, Journal of Power Sources 115 (2003) 171–178.
[19] G.H. Brilmyer, W.H. Tiedemann, US Patent 4876513, 1989.
[20] A. Jossen, Journal of Power Sources 154 (2006) 530–538.
[21] E. Meissner, G. Richter, Journal of Power Sources 144 (2005) 438–460.
[22] S. Peck, M. Pierce, Development of a Temperature-Dependent Li-ion Battery Thermal Model, SAE Technical Paper 2012-01-0117, 2012. http://dx.doi.org/10.4271/2012-01-0117.
[23] K. Lahiri, S. Dey, D. Panigrahi, A. Raghunathan, Design Automation Conference, in: 15th International Conference on VLSI Design IEEE Computer Society (2002). p. 261.
[24] L. Song, J.W. Evans, Journal of the Electrochemical Society 147 (2000) 2086.
[25] M. Doyle, T.F. Fuller, J. Newman, Journal of the Electrochemical Society 140 (1993) 1526.
[26] T.F. Fuller, M. Doyle, J. Newman, Journal of the Electrochemical Society 141 (1994) 982.
[27] T. Evans, T. Nguyen, R.E. White, Journal of the Electrochemical Society (1989) 328.
[28] K.C. Tsaur, R. Pollard, Journal of the Electrochemical Society 131 (1984) 975.
[29] W. Gu, C. Wang, Journal of the Electrochemical Society 147 (2000) 2910–2922.
[30] W. Gu, C. Wang, J.W. Weidner, R.G. Jungst, G. Nagasubramanian, Journal of the Electrochemical Society (2000) 427.
[31] K.C. Syracuse, W.D.K. Clark, Annual Battery Conference on Applications and Advances, IEEE, California State University, Long Beach, CA, USA, 1997, pp. 163–170.
[32] M. Pedram, Q. Wu, in: Proceedings 1999 Design Automation Conference ACM (1999), pp. 861–866.
[33] S. Gold, in: The Twelfth Annual Battery Conference on Applications and Advances, IEEE, 1997, pp. 215–222.
[34] T. Panigrahi, D. Panigrahi, C. Chiasserini, S. Dey, R. Rao, A. Raghunathan, K. Lahiri, in: Proceedings of the The 14th International Conference on VLSI Design, IEEE, 2001, pp. 57–63.
[35] B.G. Pollet, I. Staffell, J.L. Shang, Electrochimica Acta 84 (2012) 235–249, ISSN 0013-4686, http://dx.doi.org/10.1016/j.electacta.2012.03.172.
[36] D.L. Anderson, Duke University, 2009.
[37] Tsinghua University.http://www.transportation.anl.gov, 2010.
[38] M. Venis.marc@vencon.com, November 2011.
[39] A.V. Oppenheim, R.W. Schafer, J.R. Buck, Discrete-time Signal Processing, Prentice Hall Upper Saddle River (1989).
[40] E. Kriss, Chinese Battery Manufacturing, Fair Isle Press, 2011.